Tellus (1999), 51A, 630–651
Printed in U K. All rights reserved

TELLUS
ISSN 0280–6495

GCM experiments to test a proposed dynamical stabilizing mechanism in the climate system

By V. A. ALEXEEV* and J. R. BATES, *Danish Center for Earth System Science, Niels Bohr Institute for Astronomy, Physics and Geophysics, University of Copenhagen, Juliane Maries Vej 30, DK-2100 Copenhagen Ø, Denmark*

(Manuscript received 18 September 1998; in final form 10 May 1999)

ABSTRACT

A dynamical mechanism of sufficient strength to maintain the stability of the observed annual mean global climate against the destabilizing influence of the positive lower tropospheric water vapour/infrared radiative (WVIR) feedback on SST perturbations has recently been proposed (Bates, 1999). The mechanism consists of an evaporative negative feedback associated with the atmospheric angular momentum (AM) cycle and the surface winds which it induces. The mechanism was found from an analysis of a simple two-zone model of the climate system. Numerical experiments with an atmospheric GCM aimed at testing the conclusions of the simple model are here described. Aquaplanet boundary conditions with a prescribed latitudinally-varying SST distribution are adopted. An equinoctial distribution of solar radiation is assumed. An equilibrium climate for the GCM is established and perturbation experiments with a uniform 2 K increase in the SST are carried out. In the equilibrium and basic perturbation experiments, the GCM is run with all fields evolving freely. Further perturbation experiments are then carried out with the cloud fields held fixed, and with both the cloud and water vapour fields held fixed, in the GCM's radiation package. These experiments allow the relative influence of cloud and water vapour in the infrared and solar radiative feedbacks at the surface to be estimated. The results of the experiments are compared with those predicted by the simple model for a similar SST perturbation. The GCM results are found to be consistent with the basic assumptions and conclusions of the simple model. In particular, they indicate that a positive WVIR feedback exists in both the tropical and extratropical zones and confirm the existence of a negative evaporative feedback associated with the AM cycle that is of sufficient strength to overcome it. The experiments support the conclusion based on the simple model that it is necessary to consider both the wind factor and the humidity factor in evaluating the evaporative feedback. The cloud/infrared radiative feedback in the GCM is found to be small compared with the WVIR feedback. The experiments suggest that the feedback resulting from the absorbtion of solar radiation by water vapour (which was not included in the simple model) provides a significant additional stabilizing influence on SST perturbations.

1. Introduction

A remarkable feature of the Earth's climate is its stability on long time scales. The global mean surface temperature varies very little over millennia despite the existence of potentially destabilizing feedbacks such as the lower tropospheric WVIR feedback and the ice-albedo feedback. In the scientific literature, the question of climate stability has been addressed mainly in the context of simple climate models and of individual physical processes such as cloud-radiation.

Recently, a dynamical stabilizing mechanism in the climate system based on atmospheric AM

* Corresponding author.
e-mail: boba@dcess.ku.dk

transport and the surface winds and evaporation which it induces has been proposed (Bates, 1999 — hereinafter B99; see the introduction of that paper for a general discussion of the question of climate stability; see also Clement and Seager (1999), Larson et al. (1999), and references therein). The stabilizing mechanism in question was found from an analysis of a simple two-zone model of the climate system. The model employs ocean energy equations with the surface fluxes calculated explicitly and with the poleward ocean heat transport included. The AM transport is seen in the model as a much more important agent of interaction between the tropical and extratropical oceans than the heat transport by ocean currents, since the surface latent heat fluxes induced by the former in both zones are much greater than the inter-zone energy coupling due to the latter. The AM transport is parameterized using an empirical relationship derived from seasonal mean observations. This shows that the vertically integrated transport across 30° is directly related to the difference between the mean heights of the 500 hPa surface in the tropics and the extratropics, which is a gross measure of the baroclinicity. The sensitivity of the tropical 500 hPa height to SST perturbations is parameterized using an assumption of a moist adiabatic lapse rate, while that of the extratropical height is parameterized using an empirical formula derived from seasonal mean observations. In calculating the turbulent fluxes, surface winds derived from considerations of AM transport and torque balance are used, with the low-level relative humidity and air–sea temperature difference constrained to remain fixed at their observed mean values. The model's equilibrium temperatures are prescribed and the equilibrium surface fluxes are calculated using the above assumptions. The calculated fluxes show good agreement with observation. The equilibrium climate is then perturbed and an analytical solution for the evolution of the perturbations is obtained. This gives rise to stability criteria (the conditions for the decay of the two normal modes of the model) which depend on the sensitivities of the surface fluxes. These, in turn, depend on the mean fluxes and involve the AM transport and its sensitivity. It was found that the tendency toward instability resulting from the WVIR feedback is overcome by the evaporative flux sensitivities, with the sensible heat flux and ocean heat transport sensitivities playing minor rôles. The physical processes involved in the negative feedback mechanism are clearly evident in the case of a globally uniform SST perturbation. In that case, an increase in the tropical–extratropical 500 hPa height difference occurs due to the greater sensitivity of the height in the tropical zone. The AM transport and surface winds then increase, and the evaporation increases due to both the wind and humidity factors (which can be of comparable magnitude, depending on the form of the perturbation), leading to a negative feedback on the initial perturbation. For other forms of initial perturbation the physics of the stabilizing mechanism is not transparent, but a detailed analysis of the model shows that the stabilizer is effective for arbitrary forms of initial perturbation as long as the normal mode stability criteria are satisfied. Since both the wind and humidity factors in the evaporative sensitivities involve the AM transport, the mechanism is referred to as a dynamical stabilizer.

Our purpose in the present paper is to test the proposed stabilizing mechanism using an atmospheric GCM. We adopt the simple approach of using an aquaplanet with prescribed SSTs; since our aim is to concentrate on the essentials of the dynamical stabilizing mechanism, we do not wish to complicate the picture by including orography, land surface processes or ice-albedo effects. We use an equinoctial distribution of incident solar radiation. The diurnal cycle of solar radiation is retained, though this could easily have been replaced by a mean diurnal radiation. Guided by the simple model, we conceptually divide the planet into two zones, a tropical zone stretching from the equator to 30° and an extratropical zone stretching from 30° to the pole. Attention is focussed on the 2-year means of the angular momentum transport between the zones and of the area-integrated surface energy fluxes in each zone. (Averages of the corresponding northern hemisphere and southern hemisphere quantities are used in all cases.)

Our first task is to establish an equilibrium climate for the GCM. This is done by using a latitudinally-varying SST distribution derived from observations and varying the surface albedo until the time-mean surface energy fluxes are in equilibrium, i.e., the fluxes integrate globally to zero. (When this is the case, the time-mean energy fluxes at the top of the atmosphere must also necessarily integrate to zero — within the numerical and physical errors in the formulation of the GCM). The equilibrium climate obtained shows good agreement with many aspects of the observed climate, including the distribution of the absorbed solar radiation between the zones and the way in which the absorbed radiation is balanced by the individual surface cooling components and the implied inter-zone ocean heat transport. The AM transport between the zones in the GCM's equilibrium climate is found to be considerably greater than that observed in the Northern Hemisphere (and used in the simple model), but quite close to that observed in the Southern Hemisphere. Overall, the equilibrium climate has sufficient similarity with the observed climate, and with the equilibrium climate of the simple model, to allow it to be used as the basis of our climate perturbation experiments.

In the perturbation experiments, the SST is increased uniformly by 2 K over the globe and the consequent changes in the GCM's time-mean angular momentum transport and surface fluxes are examined. In choosing a 2 K perturbation we were guided by the example of Randall et al. (1992) and Cess et al. (1996), who studied aspects of climate sensitivity in GCMs subject to a ± 2 K SST perturbation. The simple model predicts that, for a stable equilibrium climate, the initial SST tendency for the chosen form of perturbation (but not for all forms of perturbation) about equilibrium will be negative in each zone. Since our GCM is not coupled with an interactive ocean model, its feedback tendencies are evaluated in terms of the changes that develop in the surface fluxes as a result of the imposed SST perturbation. In addition to the feedbacks which were included in the simple model, the GCM allows the possibility of cloud-radiative feedbacks and of a water vapour feedback on the solar radiation absorbed at the surface. As well as the basic climate perturbation experiment described above, additional experiments are performed to assess the separate contributions of cloud and water vapour to the infrared and solar radiative feedbacks at the surface.

The equilibrium and perturbed climates of the GCM are compared with those of the simple model and details of the various components that make up the simple model are examined in the light of the GCM results. We relate our globally averaged results to those of Randall et al. loc. cit., who intercompared the global surface energy fluxes in a large number of GCMs under conditions of a perturbed SST.

The reader is referred to Section 7 for a list of definitions of the symbols and abbreviations used in our paper.

2. Model description

The model used is an atmospheric GCM on an aquaplanet with prescribed latitudinally-varying SSTs. The dynamical core of the GCM is that developed by Bates et al. (1993) and Moorthi et al. (1995). It uses a two-time-level semi-Lagrangian semi-implicit finite difference integration scheme with a regular latitude-longitude grid and a sigma vertical coordinate. The physical parameterization package is the GEOS package described by Takacs et al. (1994); the turbulence parameterization is that developed by Helfand and Labraga (1988), the convective parameterization is the relaxed Arakawa–Schubert scheme of Moorthi and Suarez (1992), and the longwave and shortwave radiation schemes closely follow those of Harshvardhan et al. (1987). The turbulent eddy fluxes of momentum, heat and moisture in the surface layer are calculated using stability-dependent bulk formulae based on Monin–Obukhov similarity functions. The model is run at a resolution of $2^\circ \times 2.5^\circ$ with 20 vertical levels and a 1 h timestep for the dynamics. The GCM in this configuration has been tested for climate simulation (Chen and Bates, 1996) and has been found to give good results.

The reference SST field used in the present aquaplanet experiments, shown in Fig. 1, is obtained by taking annual mean observations, performing zonal averaging, symmetrizing with respect to the equator, performing some smoothing and replacing negative values (less than $0\,^\circ$C) by zero. Since we are not concerned here with the ice-albedo feedback, no sea ice is included in the model. A perturbed SST field is defined by everywhere adding 2 K to the reference field. The insolation is prescribed at its equinoctial distribution, with the diurnal cycle retained, and the surface albedo is prescribed at a uniform value of 0.15. This value was chosen by initial experimenta-

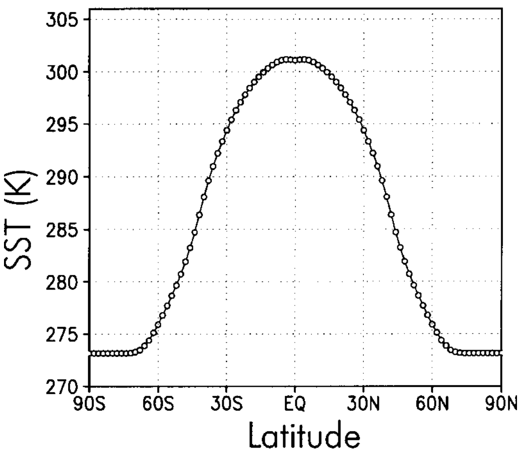

Fig. 1. The reference SST field.

tion so as to give a climate in approximate equilibrium when the reference SST distribution is used.

3. Two-year integrations

A number of experimental 2-year integrations of the GCM are carried out with the SST field set at its reference and perturbed distributions. The aim of the experiments is to study feedback tendencies by examining the model's response to the SST perturbation. Actual feedbacks on the SST are not permitted in our experiments, since the SST is fixed. The feedback tendencies indicate what would happen if the SST were free to respond to the induced surface fluxes. For simplicity of description, we refer to feedback tendencies as feedbacks.

The SST feedbacks in question are:

(i) The WVIR feedback
(ii) The cloud/IR radiative feedback
(iii) The water vapour/solar radiative feedback
(iv) The cloud/solar radiative feedback
(v) The evaporative feedback
(vi) The sensible heat flux feedback

The approach used is to examine the changes that occur in the 2-year time-mean surface fluxes in the tropical (0°–30°) and extratropical (30°–90°) zones, referred to as zones 1 and 2, respectively, on going from the reference to the perturbed SST distribution, using variations of the model code. The results presented for zones 1 and 2 are averages of the two area-integrated values obtained for the corresponding northern hemisphere and southern hemisphere zones (it was found that there was little asymmetry between hemispheres).

A 6-month spin-up integration starting from an ECMWF analysis projected on to the model levels without orography is first performed, with the SST set at its reference distribution and with all model fields allowed to evolve freely. In the early part of the spin-up period, significant trends in the surface fluxes in both zones and in the AM transport between zones were evident. By the end of the period these trends had disappeared, but the fluxes (particularly of latent heat and AM) continued to show considerable month-to-month variability. The atmospheric state produced at the end of this spin-up period is designated S1. Six experimental 2-year integrations are then performed. The experiments, described in detail below, are summarized in Table 1.

In experiment 1, the model integration is continued for 2 years from the state S1, under the same conditions as above. This is taken as the basic equilibrium climate experiment. Using standard error estimates based on monthly means (see Section 8 for details), it was found that the 2-year integration period was sufficient to give reliable estimates of the mean fluxes. The average zonal-mean cloud and specific humidity fields from the first 6 months of experiment 1, symmetrized about

Table 1. *The 2-year GCM experiments*

Experiment	1	2	3	4	5	6
initial state	S1	S2	S3	S4	S5	S6
SST perturbation	0	+2 K	0	+2 K	0	+2 K
clouds in radiation package	free	free	fixed from experiment 1	fixed from experiment 1	fixed from experiment 1	fixed from experiment 1
specific humidity in radiation package	free	free	free	free	fixed from experiment 1	fixed from experiment 1

the equator, are saved for later use. The vertical grid on which the fields are stored are the pressure levels corresponding to the model's sigma levels for a surface pressure of 1000 hPa. When used later, the fields are interpolated to the model's sigma levels corresponding to the ambient surface pressure.

In experiment 2, the SST field is set at its perturbed distribution and all model fields are allowed to evolve freely as in experiment 1. The model is first integrated for 6 months from the state S1 with the perturbed SST to produce a new spun-up state S2. (A 6 month spin-up from state S1 was used in all experiments involving a 2 K perturbation; in the other cases, a 3-month spin-up period was found to be sufficient for the initial trends to disappear). The experiment then consists of a 2-year integration proceeding from state S2.

In experiment 3, the SST is restored to its reference distribution and the cloud fields in the radiation package of the GCM code are fixed at the 6-month average zonal mean distributions provided by experiment 1. It is to be noted that even though the cloud amounts are fixed, their radiative properties (both longwave and shortwave) can still vary somewhat, since these are functions of temperature (Takacs et. al., 1994). The model is spun up for 3 months starting from state S1 under these conditions, to provide the state S3. The experiment then consisits of a 2-year integration proceeding from state S3.

In experiment 4, the SST field is set at its perturbed distribution and the model is run as in experiment 3. A 6-month spin-up from state S1 is performed to provide the state S4, and the experiment consists of a 2-year integration proceeding from state S4.

In experiment 5, the SST is restored to its reference distribution. The cloud and specific humidity fields in the radiation package of the GCM are fixed at the mean values provided by experiment 1 (in calculating the precipitation, freely evolving cloud and water vapour fields are used). The model is spun up for 3 months from state S1 under these conditions to give the state S5. The experiment consists of a 2-year integration proceeding from state S5.

In experiment 6, the SST field is set at its perturbed distribution while the cloud and specific humidity fields are treated as in experiment 5. The model is spun up for 6 months from state S1 to produce a state S6. The experiment consists of a 2-year integration proceeding from state S6.

3.1. Comparison of experiments 1 and 2

All the feedbacks listed earlier act simultaneously when we go from experiment 1 to experiment 2. For the particular type of SST perturbation being used, we expect from the simple model of B99 that, in both zones, the WVIR feedback will be positive, the latent and sensible heat flux feedbacks will be negative (with the latter small in magnitude), and the sum of the latent and sensible heat flux feedbacks will dominate over the WVIR (see Section 9). These conclusions of the simple model are based on simplified modelling assumptions which allow the relevant sensitivity parameters to be determined.

The 2-year mean surface fluxes in zones 1 and 2 and the vertically integrated eddy AM transports at 30° for experiments 1 and 2 are shown in Fig. 2. It is seen that, as required, there is an approximate global balance in the surface fluxes in the GCM's equilibrium climate (experiment 1); the solar radiation absorbed over a hemisphere is 46.13 PW while the IR and turbulent heat losses are 46.16 PW. The figures for experiment 2 show that the fluxes become unbalanced as a result of the 2 K SST perturbation; the absorbed solar radiation decreases to 45.30 PW while the combined losses increase to 46.59 PW. Thus, there is an overall negative feedback on the SST perturbation, the contribution from the absorbed solar radiation being -0.83 PW and the contribution from the combined surface losses (turbulent plus IR) being -0.43 PW. This is composed of 0.90 PW by the IR radiation flux and -1.33 PW by the turbulent fluxes. Combining the global fluxes in another way, it is seen that the radiative feedback (IR plus solar) is slightly positive ($+0.07$ PW), but it is greatly outweighed by the negative turbulent (latent plus sensible) heat flux feedbacks (-1.33 PW). The eddy AM transport at 30° (F_M) is seen to increase by 10.1% as a result of the SST perturbation. This is to be compared with the increase of 6.5% in F_M predicted by the simple model of B99 as a result of a uniform 2 K SST increase. The figures given above are statistically significant (see Section 8).

In the equilibrium climate, the magnitudes of the surface fluxes are qualitatively similar to those

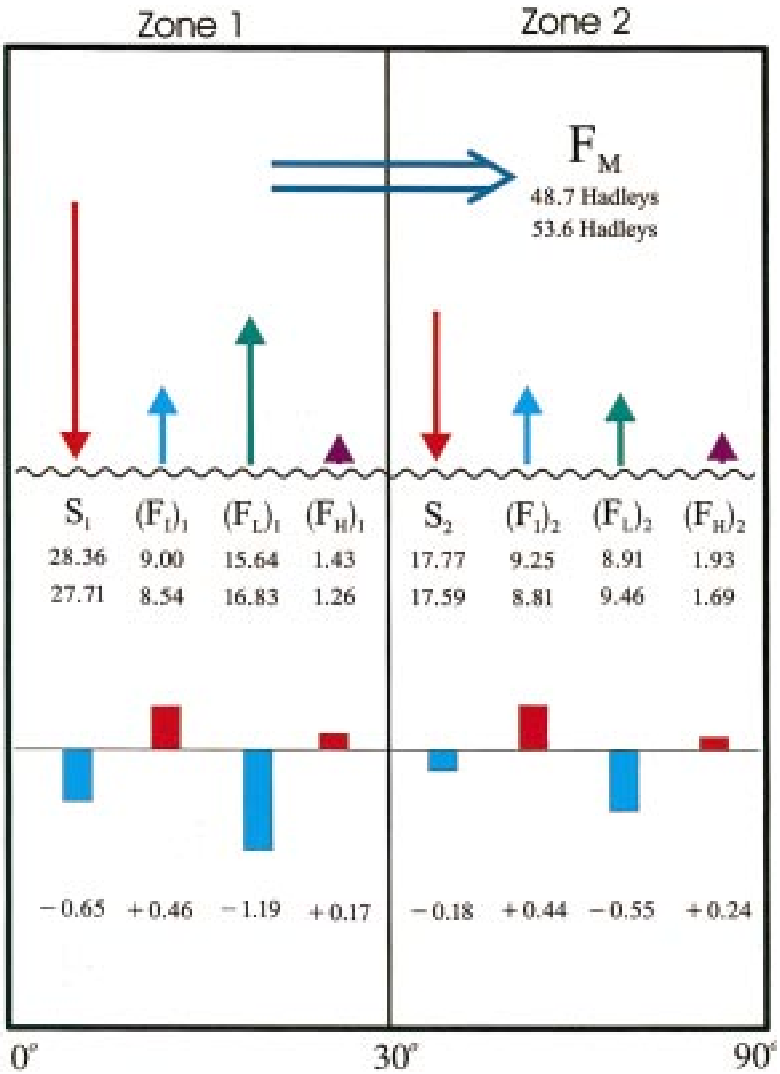

Fig. 2. Two-year mean surface fluxes (PW) and eddy AM transports (Hadleys) for experiments 1 and 2. (The upper and lower figures under the flux symbols refer to experiment 1 and experiment 2, respectively.) In the lower part of the diagram the differences in the surface fluxes between experiment 2 and experiment 1 are shown, with positive feedbacks shown above and negative feedbacks below the zero line. (S = solar flux, F_I = net upward IR flux, F_L = latent heat flux, F_H = sensible heat flux. Subscripts 1 and 2 denote zones 1 and 2. F_M = AM transport at 30°. Full definitions of symbols given in Section 7.)

in the equilibrium climate of the simple model of B99. The following specific points of similarity between the GCM results and those of the simple model are found: (a) in both cases, the primary term balancing the absorbed solar radiation is the evaporative heat loss in zone 1 and the net IR radiative heat loss in zone 2; (b) in both cases, the sensible heat losses are small by comparison with the evaporative and IR radiative heat losses; (c) the GCM has an implied ocean heat transport of approximately 2.3 PW from zone 1 to zone 2, since the absorbed solar radiation exceeds the surface losses by this amount in zone 1 and is less than the surface losses by this amount in zone 2.

This value of the ocean heat transport is very similar to the value of 2.4 PW used in the simple model. The main point of dissimilarity between the GCM equilibrium experiment and the simple model is the magnitude of F_M (48.7 Hadleys in the GCM as against 30 Hadleys in the simple model and northern hemisphere observation; however, as noted earlier, the value of F_M in the GCM is in good agreement with southern hemisphere observation).

The IR radiative feedback (cloud plus water vapour) arising from the SST perturbation is seen to be positive in zones 1 and 2, i.e., the higher temperatures lead to a reduced net IR radiative heat loss from the surface in both zones. The strength of the radiative feedback is somewhat weaker in zone 1 than the value used in B99 ($\gamma_{I1} = -0.23$ PW K^{-1} as against $\gamma_{I1} = -0.37$ PW K^{-1}) and considerably stronger in zone 2 ($\gamma_{I2} = -0.22$ PW K^{-1} as against $\gamma_{I2} = -0.04$ PW K^{-1}). It is interesting to note that if we insert these values of γ_{I1} and γ_{I2} into the stability criteria of the simple model, while keeping all other parameters as in Table 1 of B99, the criteria are still satisfied. We shall see later that the positive IR radiative feedback in the GCM is due to water vapour rather than cloud. The evaporative feedback is seen to be negative in both zones and, though smaller in magnitude than that predicted by the simple model (see Section 9), is of sufficient magnitude to overcome the positive IR radiative feedback. Unlike the case of the simple model, the sensible heat feedback in the GCM is positive in both zones. (This feedback was also found to be positive globally in the experiments of Randall et al., 1992.) Its magnitude is sufficiently small in zone 1 that, when it is added to the positive IR radiative feedback, the sum of the two is still overcome by the negative evaporative feedback. In zone 2, however, the sum of the positive sensible heat and IR radiative feedbacks outweighs the negative evaporative feedback, and the solar radiative feedback (which is negative in both zones) is needed to give a combined negative feedback.

The negative evaporative feedbacks are caused in part by the increased surface winds resulting from the increased AM transport and in part by the increased surface humidity factor resulting from the SST increase. (Calculations aimed at assessing the relative importance of these factors will be described in Section 4.) The vertically integrated AM transports as a function of latitude for experiments 1 and 2 are shown in Fig. 3. While the maximum transports are considerably larger than those given by northern hemisphere observations, the general character of the transports is in good agreement with observation, particularly for the southern hemisphere. The eddy transports are dominant and attain their maximum values in the neighbourhood of 30°, where the transports by the mean meridional motion are close to zero. The latitudes of maximum eddy transport and of zero mean meridional transport change only very slightly as a result of the SST perturbation. While,

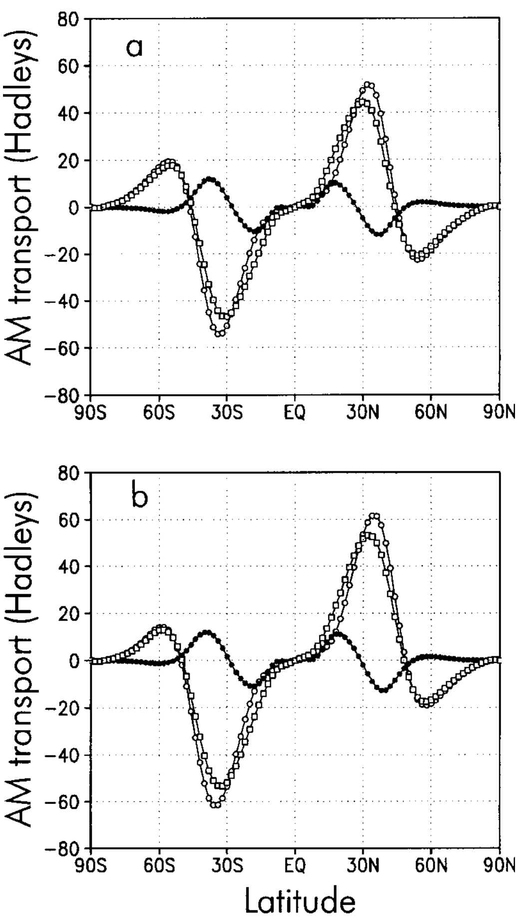

Fig. 3. Temporally and zonally averaged vertically-integrated meridional AM transport as a function of latitude (squares, total transport; open circles, eddy transport; dark circles, transport by mean meridional circulation). (a) Experiment 1; (b) experiment 2.

as we have seen, the eddy transport at 30° (F_M) increases by 10.1%, the total transport at 30° increases by 17.8% as a result of the perturbation, going from 43.96 to 51.77 Hadleys. (The maxima of the eddy and total transports increase by 19.5% and 20.7%, respectively.)

The 500 hPa height fields for experiments 1 and 2 as a function of latitude are shown in Fig. 4. The average height in zone 1 (Z_1) increases from 5826 m to 5892 m as a result of the SST perturbation, while the average height in zone 2 (Z_2) increases from 5397 m to 5449 m. If we regard the increase in each zone as being due to the SST increase in that zone, we have

$$\left(\frac{dZ_1}{dT_{S1}}, \frac{dZ_2}{dT_{S2}}\right) = (33, 26)\ \mathrm{m\ K^{-1}}. \quad (1)$$

These values, as well as being greater than, are closer together than the values (28.4, 17.8) m K^{-1} determined in B99 on the basis of moist adiabatic ascent for zone 1 and observed seasonal variations in the 1000–500 hPa thickness at 50°N for zone 2. While the change in the tropical–extratropical 500 hPa height difference (ΔZ_{500}) resulting from a uniform 2 K SST increase is less in the GCM (14 m) than in the simple model (21 m), the resulting increase in F_M is actually greater in the GCM than in the simple model (10.1% compared to 6.5%, as noted earlier), and the increase in the GCM's total AM transport at 30° is greater still.

Fig. 5 shows the latitudinal distributions of the zonal means of the absolute value of the zonal wind at 10 m ($|\bar{u}_{10}|$) and the total surface stress ($\bar{\tau}$). It can be seen that the two quantities vary in a very similar manner and that their proportional variations from experiment 1 to experiment 2 are similar. The latter quantity is closely related to the total mean surface fluxes. In the simple model of B99 we have used $|\bar{u}_{10}|$ in conjunction with the bulk aerodynamic formulae to calculate the total surface fluxes. The results shown in Fig. 5 provide support for the approximation used in the simple model as far as variations in the total surface fluxes is concerned.

Fig. 6 shows the latitudinal distribution of the

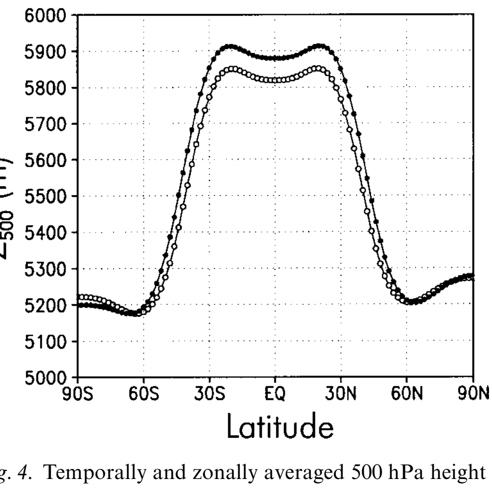

Fig. 4. Temporally and zonally averaged 500 hPa height ($\bar{Z}_{500}$) as a function of latitude for experiment 1 (open circles) and experiment 2 (dark circles).

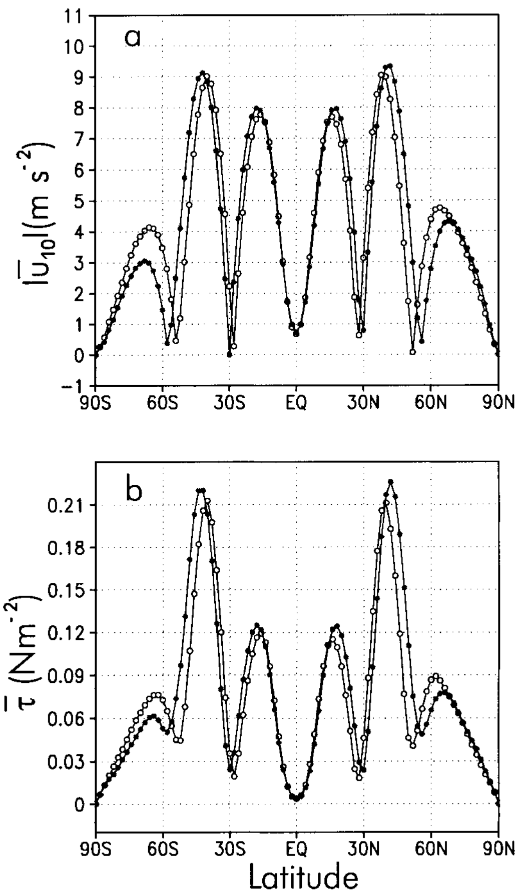

Fig. 5. (a) Temporal and zonal average of the magnitude of the zonal wind component at 10 m ($|\bar{u}_{10}|$) as a function of latitude for experiment 1 (open circles) and experiment 2 (dark circles). (b) As in (a), except for total surface stress ($\bar{\tau}$).

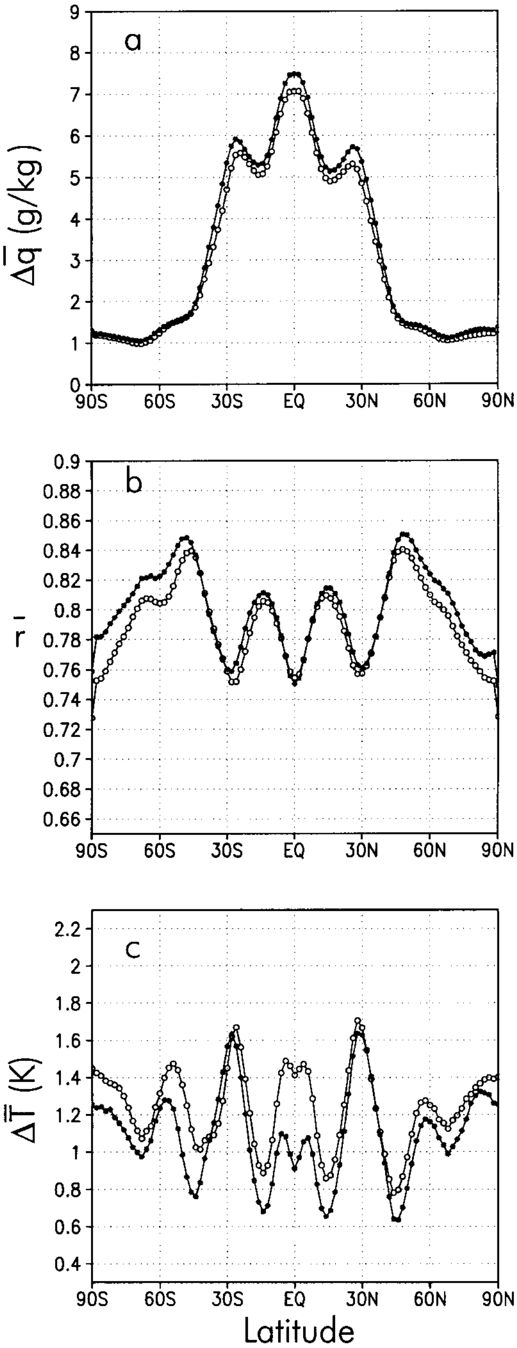

Fig. 6. Latitudinal distributions of the temporally and zonally averaged values of (a) the surface humidity deficit ($\Delta\bar{q}$), (b) the relative humidity at 10 m ($\bar{r}$), and (c) the air–sea temperature difference ($\Delta\bar{T}$). Experiment 1, open circles; experiment 2, dark circles.

zonal mean surface humidity deficit ($\Delta\bar{q}$), the zonal mean relative humidity at 10 m ($\bar{r}$), and the zonal mean air–sea temperatue difference ($\Delta\bar{T}$), for experiments 1 and 2. It can be seen that $\Delta\bar{q}$ increases slightly as a result of the perturbation (mainly in the lower latitudes), $\bar{r}$ remains almost constant over most of the globe (its global mean increases from 0.79 to 0.80), and $\Delta\bar{T}$ decreases slightly (its global mean goes from 1.23 K to 1.06 K). These values of $\bar{r}$ and $\Delta\bar{T}$ are very similar to the global values of r (0.8) and ΔT (1 K) adopted in B99 on the basis of observations. Constancy of the relative humidity under perturbation of the climate has also been found in the GCM experiments of Randall et al. (1992) and in experiments on CO_2 doubling (Bengtsson, 1998). The latent heat fluxes as a function of latitude are shown in Fig. 7. While the area-averaged fluxes increase in both zones as a result of the SST perturbation, it is seen that the principal increase occurs in zone 1.

It is of interest to compare the rates of change with SST of the globally averaged surface fluxes given by our experiments 1 and 2, and by those of the simple model of B99, with those given by Randall et al. (1992). To carry out the comparison, we take the flux increments for the simple model from Section 9 of the present paper; the increments for zones 1 and 2 corresponding to a 2 K SST perturbation are given by eq. (C.4). In the case of the Randall et al. results, we use the mean flux increments for a 4 K SST increase given on p. 3720 of their paper. Adopting the notation of Randall et al. for the purpose of the comparison, the globally averaged net downward flux per unit area at the surface is given by

$$N = \mathrm{SW} + \mathrm{LW} + \mathrm{SH} + \mathrm{LH} \qquad (2)$$

where SW, LW, SH and LH denote the shortwave, longwave, sensible heat and latent heat fluxes, respectively. (The sign convention adopted in (2), with positive values denoting fluxes into the surface, is such that positive/negative rates of change correspond to positive/negative feedbacks on SST perturbations.) The rates of change of the various flux components are given in Table 2.

It can be seen that in all cases the longwave feedback is positive and that it is easily outweighed by the negative evaporative feedback (and by the sum of the evaporative and sensible heat feedbacks). Our experiments 1 and 2 also show a

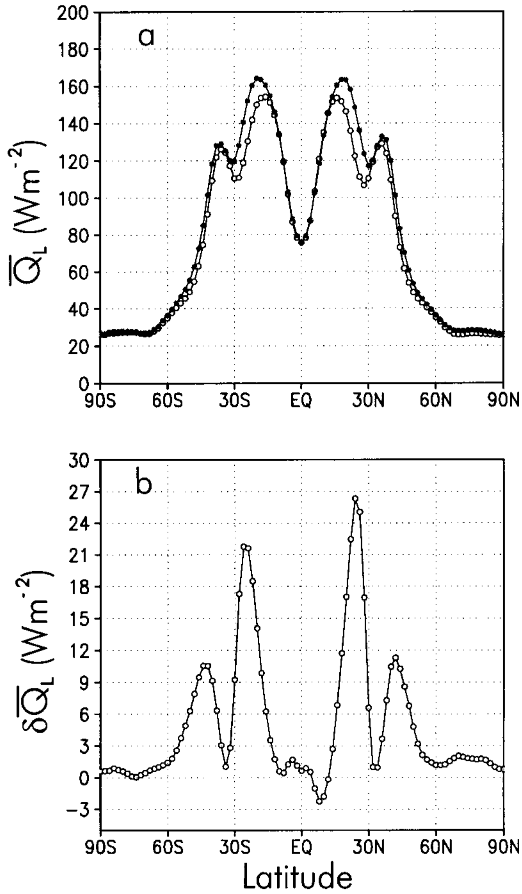

Fig. 7. (a) Temporally and zonally averaged latent heat flux per unit area ($\bar{Q}_L$) as a function of latitude for experiment 1 (open circles) and experiment 2 (dark circles). (b) Difference in $\bar{Q}_L$ ($\delta\bar{Q}_L$) between experiment 2 and experiment 1.

Table 2. *Rates of change with SST of the globally averaged surface flux components as given by our experiments 1 and 2, the GCM experiments of Randall et al. (1992) and the simple model of B99 (units: $Wm^{-2}K^{-1}$)*

	Experiments 1 and 2	Randall et al. (1992)	B99 model
$\Delta N/\Delta T_S$	−2.48	−1.90	−4.98
$\Delta(SW)/\Delta T_S$	−1.63	0.10	0
$\Delta(LW)/\Delta T_S$	1.76	0.82	1.61
$\Delta(SH)/\Delta T_S$	0.80	0.44	−0.12
$\Delta(LH)/\Delta T_S$	−3.41	−3.04	−6.47

significant shortwave negative feedback; this is at variance with the small positive shortwave feedback of Randall et al., though it should be noted that one of the GCMs used in the Randall et al. study (the ECMWF model) showed a negative shortwave feedback even larger than ours. All the flux sensitivities for our experiments 1 and 2 listed in Table 2 lie within the range of values given by the individual GCMs of the Randall et al. study. The same applies to the SW and LW flux sensitivities of the B99 model listed in Table 2, but not to the SH, LH or N flux sensitivities, which lie somewhat outside the range of values found in the Randall et al. study.

3.2. *Comparison of experiments 3 and 4*

Our purpose in this section and the next is to assess the relative contribution of cloud and water vapour to the radiative feedbacks found in Subsection 3.1. In the present section, the main cloud feedbacks (those depending on cloud amount) are omitted, while the water vapour feedbacks continue to act.

The 2-year mean surface fluxes in zones 1 and 2 and the vertically integrated eddy AM transports at 30° for experiments 3 and 4 are shown in Fig. 8. It is seen that in experiment 3, the hemispheric values of the absorbed solar radiation and combined surface losses are 49.49 PW and 50.24 PW, respectively; thus, while both values have increased compared to those of experiment 1, there is still a close approximation to equilibrium. The figures for experiment 4 show that as a result of the SST perturbation the absorbed solar radiation decreases slightly to 48.97 PW while the combined losses increase slightly to 50.69 PW. There is again an overall negative feedback on the SST perturbation, with the absorbed solar component slightly greater than the surface loss component component. The eddy AM transports in experiments 3 and 4 are considerably reduced from the values found in experiments 1 and 2; it appears that fixing the clouds has reduced the level of baroclinic wave activity. The eddy AM transport at 30° (F_M) is seen to increase by 5.4% as a result of the SST perturbation.

The IR radiative feedback arising from the SST perturbation is seen to be positive in both zones. The evaporative feedback is seen to be negative in both zones and of sufficient magnitude to

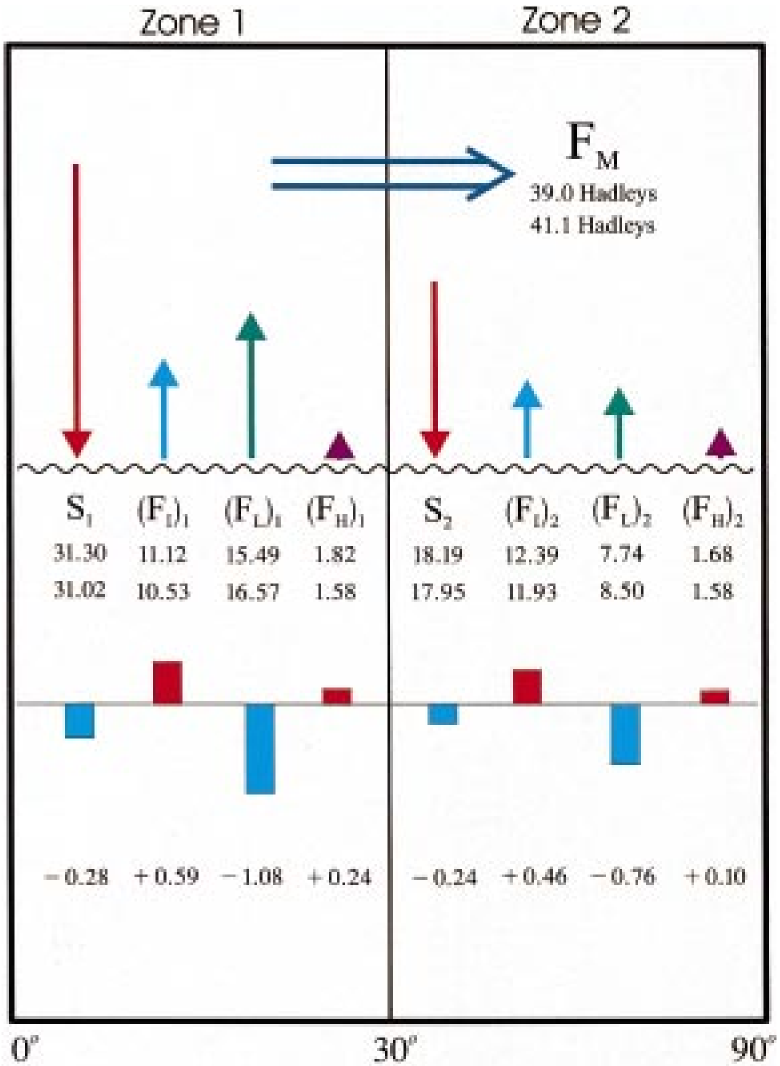

Fig. 8. Two-year mean surface fluxes (PW) and eddy AM transports (Hadleys) for experiments 3 and 4. (The upper and lower figures under the flux symbols refer to experiment 3 and experiment 4, respectively.) In the lower part of the diagram the differences in the surface fluxes between experiment 4 and experiment 3 are shown, with positive feedbacks shown above and negative feedbacks below the zero line. (Symbols as in Fig. 2.)

overcome the IR radiative feedback. The magnitudes of the IR and evaporative feedbacks are comparable to those of Subsection 3.1. The sensible heat feedback is seen to be positive in both zones, but its magnitude is sufficiently small that when it is added to the positive IR radiative feedback the sum of the two is overcome by the negative evaporative feedback. The solar radiative feedback is again negative in both zones.

The vertically integrated AM transports as a function of latitude are shown in Fig. 9. The general character of the transport components is very similar to that of Fig. 3. The latitudes of maximum eddy transport and of zero mean meridional transport again change only very slightly as a result of the SST perturbation. While, as we have seen, the eddy AM transport at 30° (F_M) increases by 5.4%, the total transport at 30°

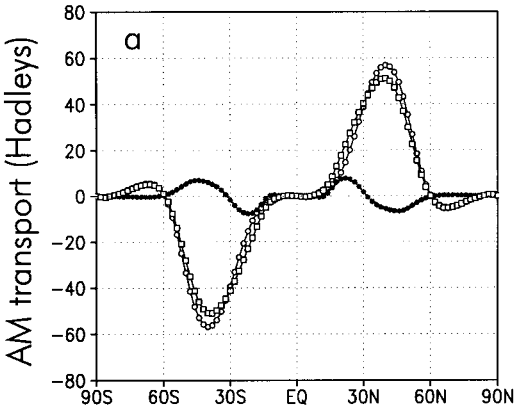

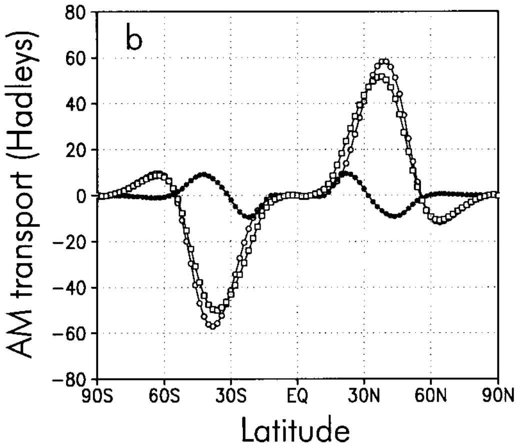

Fig. 9. Temporally and zonally averaged vertically-integrated meridional AM transport as a function of latitude (squares, total transport; open circles, eddy transport; dark circles, transport by mean meridional circulation). (a) Experiment 3; (b) experiment 4.

increases by 6.4% as a result of the SST perturbation. (The value of the maximum eddy transport increases by 1.4% while that of the maximum total transport decreases by 0.4%.)

The 500 hPa height fields for experiments 3 and 4 as functions of latitude are shown in Fig. 10. The average height in zone 1 (Z_1) increases from 5791 m to 5849 m as a result of the SST perturbation, while the average height in zone 2 (Z_2) increases from 5388 m to 5443 m. Regarding the increase in each zone as being due to the SST increase in that zone, we find

$$\left(\frac{dZ_1}{dT_{S1}}, \frac{dZ_2}{dT_{S2}}\right) = (29, 27)\ \mathrm{m\ K^{-1}}. \quad (3)$$

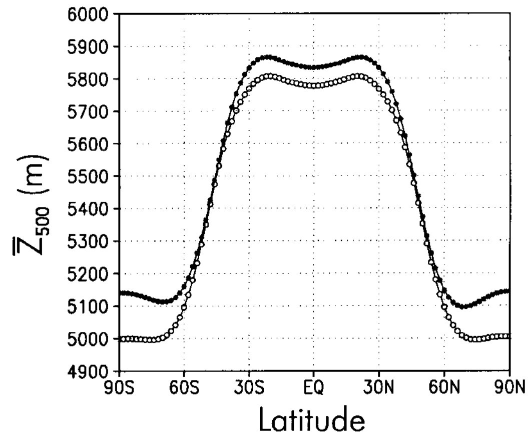

Fig. 10. Temporally and zonally averaged 500 hPa height as a function of latitude for experiment 3 (open circles) and experiment 4 (dark circles).

Comparing eq. (3) with eq. (1), we see that when the clouds are fixed the sensitivity of the tropical 500 hPa height to SST variations is no longer as great as when the clouds were evolving freely. The difference between the mean 500 hPa heights in the tropical and extratropical zones (ΔZ_{500}) increases by only 3 m (from 403 m to 406 m) as a result of the perturbation. The mean latent heat fluxes are shown in Fig. 11. While the fluxes increase in both zones as a result of the SST perturbation, it is again seen that the principal increase occurs in zone 1.

3.3. Comparison of experiments 5 and 6

In this case, with both the specific humidity and cloud fields fixed in the GCM's radiation package, there is no water vapour radiative feedback (IR or solar) and only a small cloud radiative feedback (that due to the temperature dependence of the cloud radiative properties). The surface fluxes and AM transport for the two experiments are shown in Fig. 12. In experiment 5 the hemispheric value of the solar radiation absorbed at the surface is 49.26 PW while the combined surface losses are 49.34 PW. Thus, there is again approximate equilibrium. The figures for experiment 6 show that as a result of the SST perturbation the absorbed solar radiation is virtually unchanged at 49.15 PW while the combined losses increase to 51.62 PW. Thus, there is a negative feedback on the SST

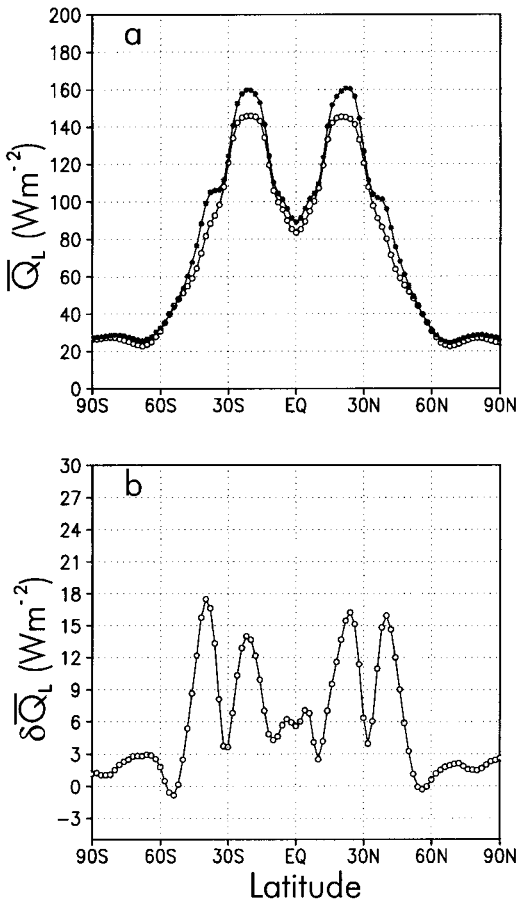

Fig. 11. (a) Temporally and zonally averaged latent heat flux per unit area ($\bar{Q}_L$) as a function of latitude for experiment 3 (open circles) and experiment 4 (dark circles). (b) Difference in $\bar{Q}_L$ ($\delta\bar{Q}_L$) between experiment 4 and experiment 3.

perturbation, with the IR radiative feedback in this case acting in the same sense as the evaporative feedback in both zones; holding the water vapour field fixed has caused the IR radiation to give a straightforward Stefan–Boltzmann feedback on the SST perturbation, in contrast to the results of both Subsections 3.1 and 3.2. The sensible heat flux feedbacks again play only a minor rôle.

The vertically integrated AM transports as a function of latitude are shown in Fig. 13. The general character of the transport components is again very similar to that of Fig. 3. Once more, the latitudes of maximum eddy transport and of zero mean meridional transport change only very slightly as a result of the SST perturbation. It is seen that the eddy AM transport at 30° in this case decreases by 3.4% as a result of the SST perturbation. The total AM transport at 30° decreases by 1.7%. (The maximum of the eddy transport increases by 1.4% and the maximum of the total transport increases by 1.6%.) The 500 hPa height fields for experiments 5 and 6 as functions of latitude are shown in Fig. 14. The average height in zone 1 (Z_1) increases from 5797 m to 5847 m as a result of the SST perturbation, while the average height in zone 2 (Z_2) increases from 5388 m to 5441 m. Hence,

$$\left(\frac{dZ_1}{dT_{S1}}, \frac{dZ_2}{dT_{S2}}\right) = (25, 26)\ \mathrm{m\ K^{-1}}. \tag{4}$$

The difference between the mean heights in the tropical and extratropical zones (ΔZ_{500}) decreases by 3m (from 409 m to 406 m) as a result of the perturbation. The decrease in ΔZ_{500} is a surprising feature for which we do not have an explanation, though the decrease in F_M accompanying the decrease in ΔZ_{500} is consistent with what is expected from the simple model of B99. It is seen from Fig. 15 that, as a consequence of the decrease in F_M, the mean zonal surface stress $\bar{\tau}_x$ shows a slight decrease. The area-integrated torque about the earth's axis goes from 41.91 Hadleys to 41.01 Hadleys in zone 1 and from -37.19 Hadleys to -35.81 Hadleys in zone 2. The mean latent heat fluxes are shown in Fig. 16. While the fluxes increase in both zones as a result of the SST perturbation, it is again seen that the principal increase occurs in zone 1. The latitudinal distribution of the flux increment $\delta\bar{Q}_L$ in Fig 16b is much flatter than in Figs. 7b and 11b. This is due to the fact that the increase in evaporation in the present case is due almost entirely to the humidity factor, whereas in the previous cases the wind factor played an important rôle.

3.4. *Water vapour versus cloud effects in the radiative feedbacks*

In the experiments discussed above, the solar and IR radiative feedbacks at the surface are determined by a combination of cloud and water vapour effects. Here we bring together the results of Subsections 3.1, 3.2 and 3.3 to estimate the relative importance of cloud and water vapour in both types of radiative feedback. The cloud effects

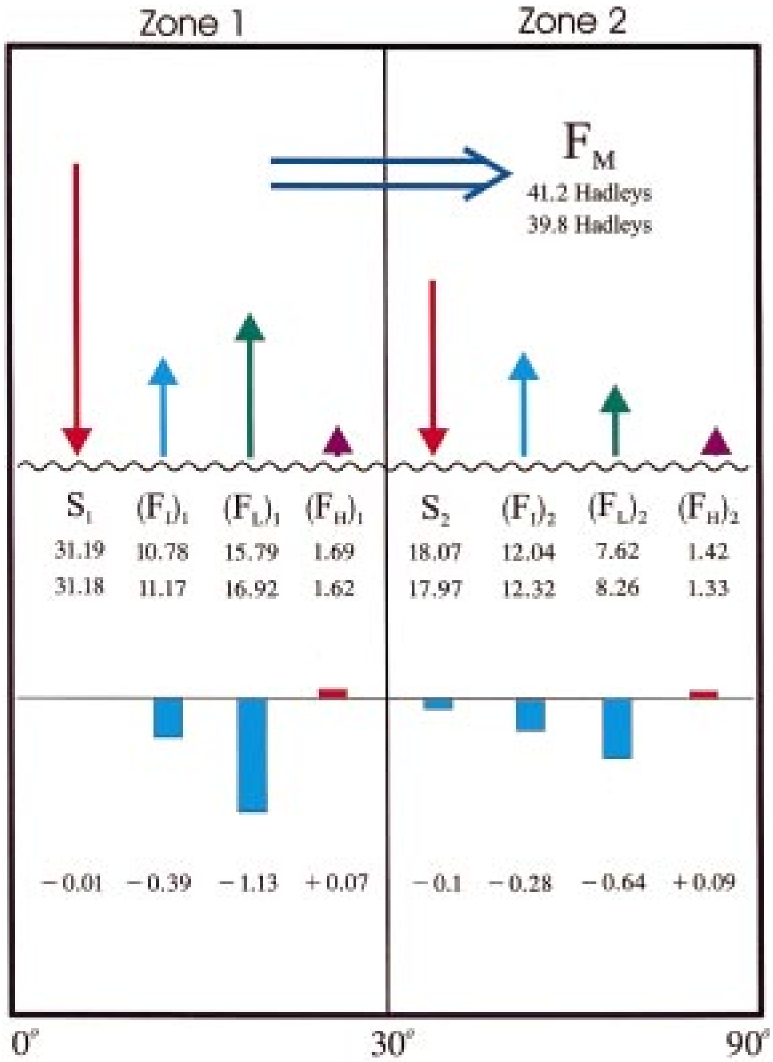

Fig. 12. Two-year mean surface fluxes (PW) and eddy AM transports (Hadleys) for experiments 5 and 6. (The upper and lower figures under the flux symbols refer to experiment 5 and experiment 6, respectively.) In the lower part of the diagram the differences in the surface fluxes between experiment 6 and experiment 5 are shown, with positive feedbacks shown above and negative feedbacks below the zero line. (Symbols as in Fig. 2.)

are estimated by taking the difference between the radiative feedbacks of Subsection 3.1 (cloud and vapour free) and Subsection 3.2 (cloud fixed and vapour free). The vapour effects are estimated by taking the difference between Subsections 3.2 and 3.3 (cloud and vapour fixed).

In the case of the solar radiation, the global feedbacks are −0.83 PW in going from experiment 1 to experiment 2, −0.52 PW in going from experiment 3 to experiment 4, and −0.10 PW in going from experiment 5 to experiment 6. Thus, the feedback due to cloud (neglecting the small effect due to cloud properties rather than cloud amount) is −0.31 PW while the feedback due to water vapour is −0.42 PW. Therefore, in the case of the solar radiative feedback both effects have the same negative sign and the vapour effect exceeds the cloud effect in the ratio 42 : 31.

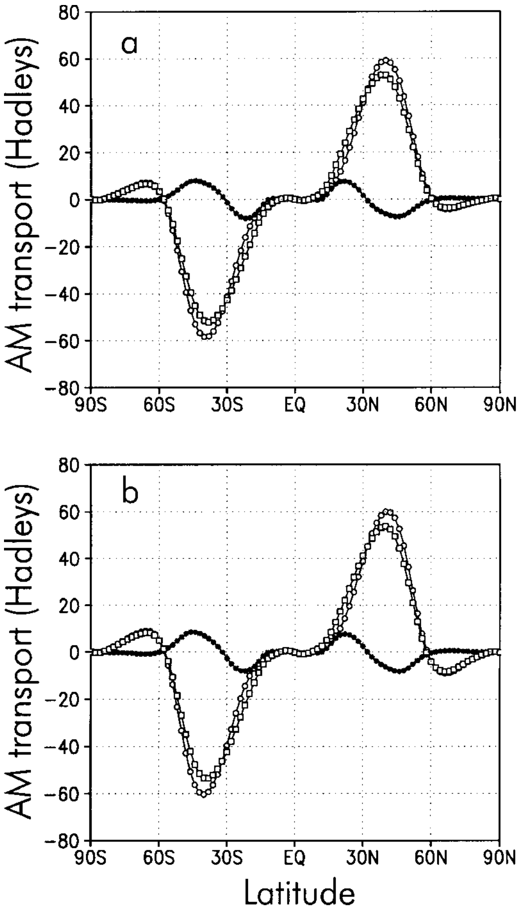

Fig. 13. Temporally and zonally averaged vertically-integrated meridional AM transport as a function of latitude (squares, total transport; open circles, eddy transport; dark circles, transport by mean meridional circulation). (a) Experiment 5; (b) experiment 6.

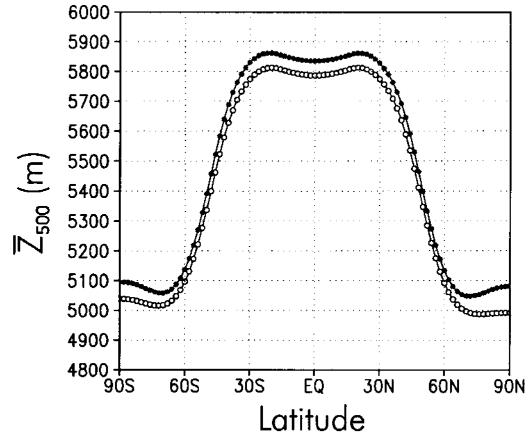

Fig. 14. Temporally and zonally averaged 500 hPa height as a function of latitude for experiment 5 (open circles) and experiment 6 (dark circles).

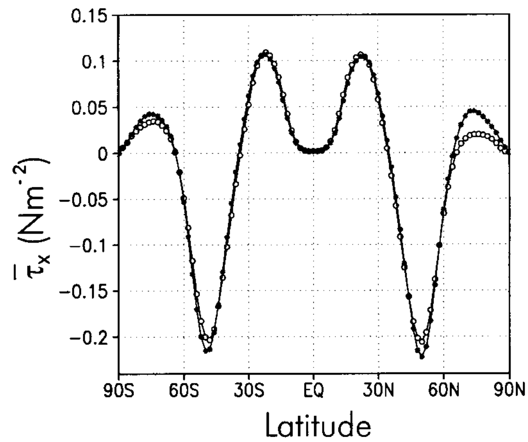

Fig. 15. Temporally and zonally averaged zonal surface stress ($\overline{\tau}_x$) as a function of latitude for experiment 5 (open circles) and experiment 6 (dark circles).

In the case of the IR radiation, the global feedbacks are +0.90 PW in going from experiment 1 to experiment 2, +1.05 PW in going from experiment 3 to experiment 4, and −0.67 PW in going from experiment 5 to experiment 6. Thus, the feedback due to cloud is −0.15 PW while the feedback due to vapour is +1.72 PW. Therefore, in the case of the IR radiative feedback, the effects have opposite sign, with the vapour feedback positive and dominant in magnitude in the ratio 172:15. Alternatively stated, the GCM experiments indicate that the positive IR radiative feedback on the SST perturbation is due to water vapour and not cloud.

4. Separating the wind and humidity factors in the evaporative feedbacks

In the integrations of experiments 1 and 2 it was seen that, in both zones, the principal factor giving a negative feedback on a uniform +2 K SST perturbation was the evaporative heat loss from the surface. As discussed in B99, this evapor-

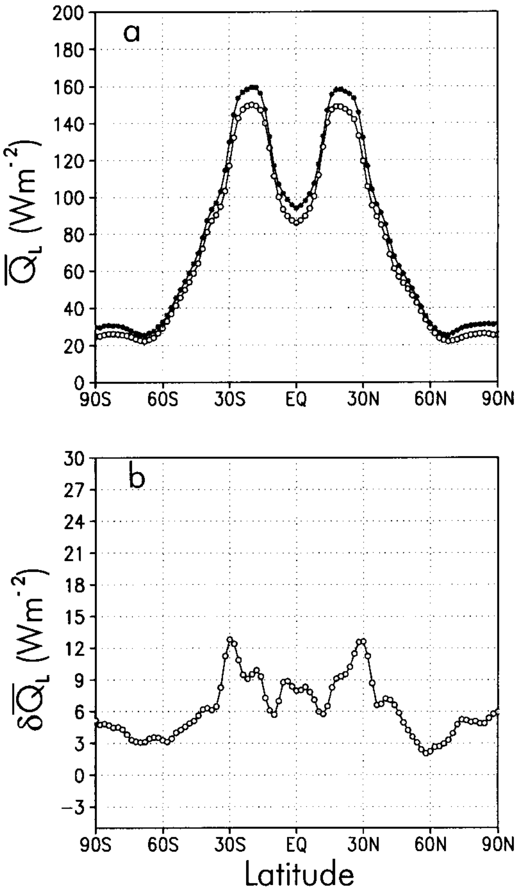

Fig. 16. (a) Temporally and zonally averaged latent heat flux per unit area ($\bar{Q}_L$) as a function of latitude for experiment 5 (open circles) and experiment 6 (dark circles). (b) Difference in $\bar{Q}_L$ ($\delta\bar{Q}_L$) between experiment 6 and experiment 5.

ative feedback can be separated into two factors, a wind factor and a humidity factor. The relative contributions of these factors which are to be expected on the basis of the simple model for the present form of SST perturbation are calculated in Section 7. It is shown that the humidity factor is expected to dominate in both zones. Here we perform some calculations aimed at separating the contributions of the wind and humidity factors to the evaporative fluxes as calculated in the GCM. Our calculations are based on the last 9 months in the integrations of experiments 1 and 2.

First, we show that the monthly-mean zonally-averaged evaporative fluxes calculated in the GCM ($(\bar{Q}_L)_{GCM}$) can be well represented by the corresponding fluxes calculated using the bulk aerodynamic formula, written as

$$(\bar{Q}_L)_{BAF} = L\rho c_E \Delta\bar{q}\bar{V}. \tag{5}$$

Here ($\Delta\bar{q}$, $\bar{V}$) represent the monthly-mean zonally-averaged values of the humidity deficit and 10-m wind magnitude, respectively, as given by the GCM. The turbulent exchange coefficient c_E is chosen so as to give the best fit to the two values of the fluxes; its value is 1.3×10^{-3} . Fig. 17 shows a scatter plot of $(\bar{Q}_L)_{GCM}$ versus $(\bar{Q}_L)_{BAF}$ using the values from all latitudes of the model grid and from both experiments 1 and 2, for the last 9 months of the integration period of each experiment. It can be seen that $(\bar{Q}_L)_{BAF}$ is a very good proxy for $(\bar{Q}_L)_{GCM}$.

Second, we show, as is to be expected from Fig. 17, that the 9-month means of the differences of $(\bar{Q}_L)_{GCM}$ and $(\bar{Q}_L)_{BAF}$ between experiments 2 and 1 (i.e., $(\delta\bar{Q}_L)_{GCM}$ and $(\delta\bar{Q}_L)_{BAF}$) are very closely related (overbars will denote 9-month means from here on). This is verified by referring to Fig. 18a, where the latitudinal distributions of $(\delta\bar{Q}_L)_{GCM}$ and $(\delta\bar{Q}_L)_{BAF}$ are shown.

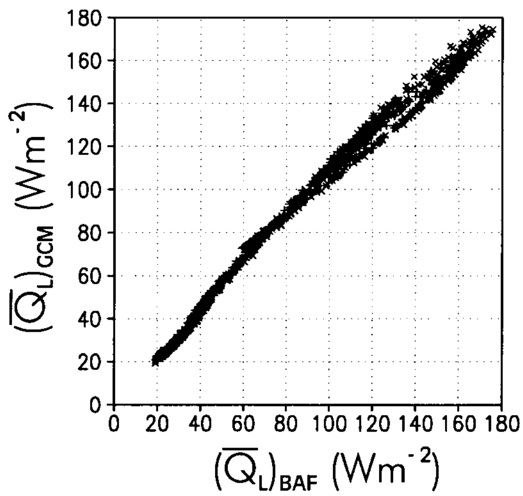

Fig. 17. Scatter plot of the individual monthly-mean zonally-averaged values of the latent heat flux per unit area as calculated in the GCM ($(\bar{Q}_L)_{GCM}$) and by the bulk aerodynamic formula ($(\bar{Q}_L)_{BAF}$). The values are obtained from the last 9 months of the integrations of experiments 1 and 2 and are calculated at all latitudes of the model grid.

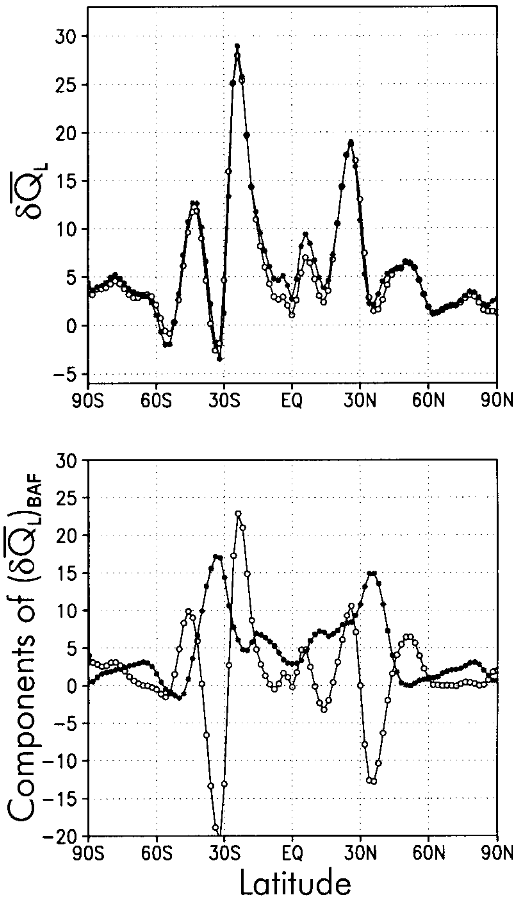

Fig. 18. (a) Differences between experiments 1 and 2 of the 9-month ensemble mean of $\bar{Q}_L$ $(\delta\bar{Q}_L)$ as a function of latitude. The open circles represent values calculated in the GCM $((\delta\bar{Q}_L)_{GCM})$ and the dark circles values calculated using the bulk aerodynamic formula $((\delta\bar{Q}_L)_{BAF})$. (b) Components of $(\delta\bar{Q}_L)_{BAF}$ as a function of latitude. The open circles represent the wind-factor component and the dark circles the humidity-factor component (units: W m^{-2}).

Third, we separate $(\delta\bar{Q}_L)_{BAF}$ into wind-factor and humidity-factor components. Using (5) we can write

$$(\delta\bar{Q}_L)_{BAF} = L\rho c_E[(\Delta\bar{q}\bar{V})_{exp2} - (\Delta\bar{q}\bar{V})_{exp1}], \tag{6}$$

where the subscripts exp1 and exp2 denote experiment 1 and experiment 2, respectively. Eq. (6) can be re-written as

$$\begin{aligned}(\delta\bar{Q}_L)_{BAF} = 0.5L\rho c_E[&\{(\Delta\bar{q})_{exp1} + (\Delta\bar{q})_{exp2}\} \\ &\times \{\bar{V}_{exp2} - \bar{V}_{exp1}\} \\ &+ \{\bar{V}_{exp1} + \bar{V}_{exp2}\}\{(\Delta\bar{q})_{exp2} - (\Delta\bar{q})_{exp1}\}].\end{aligned} \tag{7}$$

The first product within square brackets in (7) gives the wind-factor component of $(\delta\bar{Q}_L)_{BAF}$, while the second product gives the humidity-factor component. The two components are plotted as functions of latitude in Fig. 18b. In view of the similarity of $(\delta\bar{Q}_L)_{GCM}$ and $(\delta\bar{Q}_L)_{BAF}$ as demonstrated in Fig. 18a, we infer that the former partitions into wind-factor and humidity-factor components in a manner similar to that shown for the latter in Fig. 18b.

Our principal interest lies in the area-integrated flux increments in each zone resulting from the 2 K SST perturbation, since it is in terms of these that we evaluate the evaporative feedbacks. These increments are shown in Table 3. It can be seen that the components of the increments associated with the humidity factor are dominant in both zones, as predicted by the simple model, though the components associated with the wind factor are also of significant magnitude. The fact that the wind-factor component is negative in zone 2 results from a poleward movement of the wind maximum in this zone to a region in which $\Delta\bar{q}$ is smaller.

5. Conclusions and discussion

A series of GCM experiments has been carried out to test the dynamical stabilizing mechanism in the climate system proposed in B99 on the basis of a simple model. The GCM is run on an aquaplanet with a prescribed latitudinally-varying SST distribution derived from observations, and with a 2 K perturbation added to it. As in the simple model, attention is focussed on the poleward AM transport in the atmosphere and on the latent, sensible and radiative heat fluxes at the surface. Guided by the simple model, the fluxes are area-integrated for two zones, a tropical zone stretching from the equator to 30° and an extratropical zone stretching from 30° to the pole. Averages for the corresponding zones in the northern and southern hemispheres are used.

An equilibrium climate for the GCM was first determined by adjusting the surface albedo so that

Table 3. *Differences in the area-integrated fluxes of latent heat between experiment 2 and experiment 1 (PW) for zone 1, zone 2 and the two zones combined*

	GCM	BAF	BAF-wind component	BAF-humidity component
$\delta(F_L)_1$	1.23	1.34	0.52 (39%)	0.82 (61%)
$\delta(F_L)_2$	0.50	0.51	−0.22 (−43%)	0.73 (143%)
$\delta(F_L)_1 + \delta(F_L)_2$	1.73	1.85	0.30 (16%)	1.55 (84%)

The first column shows the values calculated in the GCM, the second column the values calculated using the bulk aerodynamic formula (BAF). The partitioning of the BAF values into wind and humidity components is shown in the third and fourth columns, respectively, with the corresponding percentage figures shown in brackets.

the mean surface fluxes in a 2-year integration integrated globally to zero with the prescribed (unperturbed) SST distribution. The surface fluxes for this equilibrium climate were found to be in good agreement with those of the equilibrium climate of the simple model. As in the simple model, the principal term balancing the absorbed solar radiation was found to be evaporation in the tropical zone and net IR radiation in the extratropical zone. The implied poleward ocean heat transport across the boundary of the zones in the GCM was found to be in good agreement with an estimate derived from observations and used in the simple model.

Feedbacks in the surface energy fluxes of the GCM were then studied by adding a 2 K perturbation to the equilibrium SST distribution and performing 2-year integrations. The feedbacks that occur are IR radiative feedbacks, solar radiative feedbacks (these are missing in the case of the simple model, as are cloud effects on the IR radiation), evaporative feedbacks and sensible heat feedbacks. In the basic perturbation experiment, all model fields were allowed to evolve freely. For the purpose of separating cloud and water vapour effects in the radiative feedbacks, 2-year integrations were subsequently performed with the cloud fields held fixed, and with both the cloud and water vapour fields held fixed in the GCM's radiation package, using both the equilibrium and perturbed SST distributions.

The feedbacks given by the GCM for the above SST perturbation were compared to those predicted by the simple model for the same perturbation. The basic GCM perturbation experiment gave a feedback pattern which agrees with that predicted by the simple model insofar as a central result of the simple model is concerned: the lower tropospheric WVIR feedback is positive in both zones and it is outweighed by the negative evaporative feedback linked to the AM cycle. In magnitude, the feedbacks in the GCM are also of the same order as those of the simple model. Calculations were performed to separate the wind and humidity factors in the evaporative feedbacks. It was found, as predicted by the simple model for the particular form of SST perturbation being used, that the humidity factor was dominant in both zones. (It is to be noted that since the humidity factor involves the mean zonal wind it also depends on the AM transport.) Unlike the simple model, however, the GCM experiments show that the sensible heat feedback is positive in both zones. While small in magnitude, it is nevertheless large enough that, when added to the positive WVIR feedback, the sum of the two is larger in magnitude than the negative evaporative feedback in the extratropical zone. To give an overall negative feedback in this zone, it is necessary to include the solar radiative feedback, which the GCM shows to be negative and of appreciable magnitude in both zones. The GCM results show that the IR radiative feedback is overwhelmingly due to water vapour rather than clouds, and that the solar radiative feedback is composed of comparable contributions from both factors.

The results of the GCM integrations provide support for many of the assumptions used in constructing the simple model. The following basic assumptions are qualitatively verified.

(a) The atmospheric AM transport is maximum near 30° (thus providing support for the two-zone approach, with a boundary at this latitude) and the magnitude of the transport 30° is strongly related to the difference in the mean heights of the 500 hPa surface in the tropical and extratropical zones. Large fractional changes in the AM transport across 30° occur as a result of small changes in the SST distribution.

(b) In the case of the integrations with the cloud and water vapour fields evolving freely, variations in the height of the 500 hPa surface can be determined from variations in the SST in both zones. The sensitivity is similar to that determined in the simple model, being greater in the tropical than in the extratropical zone.

(c) The mean air–sea temperature difference remains close to 1 K and the mean surface relative humidity remains close to 80% when the climate is perturbed. These two quantities, which are assumed to remain constant under climate perturbations in the simple model, are fundamental determinants of the turbulent fluxes at the surface.

Our results are similar in many respects to those of Randall et al. (1992), who studied the response of the surface fluxes in a large number of GCMs to SST perturbations. Their fluxes were not integrated according to zone, so that only globally integrated values were considered. The models used included continentality and the experiments were run for perpetual July conditions. The integration periods were much shorter than ours. The following points of agreement are found:

(a) A positive WVIR feedback occurs globally.

(b) A negative evaporative feedback occurs globally and outweighs the WVIR feedback (Randall et al. did not consider the relationship of the evaporatve feedback to the AM cycle).

(c) A positive sensible heat flux feedback occurs globally.

Unlike our case, however, Randall et al. found that the solar radiative feedback at the surface was small and positive. There was a large scatter in the results from different GCMs and the result of a positive feedback does not appear to be statistically significant. Solar radiative feedbacks are significantly dependent on the cloud radiation parameterizations, which, as emphasized by Lee et al. (1997), are still in a very uncertain state. In the case of our particular GCM, clouds exert a stabilizing influence on the SST perturbation both through the solar and IR radiation. In the course of our study, we found that the evaporative and cloud-related feedbacks varied considerably from month to month and that firm estimates of their mean values require integration periods considerably longer than those used in the Randall et al. study.

A more fundamental investigation of climate stability than we have performed here could be carried out using a coupled atmosphere–ocean model including continentality, examining how it responds to various types of perturbation in both the tropics and the extratropics. We believe that our two-zone approach and our emphasis on the effects of AM transport and its link to the surface fluxes provide a framework for meaningful interpretation of the complex results of large numerical experiments on climate stability.

6. Acknowledgments

This work was supported by the Danish National Research Foundation and the Danish National Science Research Council. The computations were performed using the facilities of the Danish Computation Centre for Research and Education (UNI·C).

7. Appendix A

Symbols and abbreviations

AM = angular momentum.

c_E = turbulent exchange coefficient for water vapour

ECMWF = European Centre for Medium Range Weather Forecasts

$(F_H)_1$ = time-mean area-integrated sensible heat flux from the ocean surface in zone 1 (average of NH and SH values)

$(F_H)_2$ = as $(F_H)_1$, but for zone 2

$(F_I)_1$ = time-mean area-integrated net (upward) IR radiative heat flux from the ocean surface in zone 1 (average of NH and SH values)

$(F_I)_2$ = as $(F_I)_1$, but for zone 2

$(F_L)_1$ = time-mean area-integrated latent heat flux from the ocean surface in zone 1 (average of NH and SH values)

$(F_L)_2$ = as $(F_L)_1$, but for zone 2

F_M = time-mean vertically-integrated poleward AM transport by transient plus stationary eddies at 30° (average of NH and SH values)
GCM = general circulation model
Hadley = unit of AM transport or area-integrated torque (1 Hadley = 10^{18} kg m^2 s^{-2})
IR = infrared
L = latent heat of vaporization of water (2.5×10^6 J kg^{-1})
NH = northern hemisphere
PBL = planetary boundary layer
PW = petawatt (10^{15} watt)
q = specific humidity
q_A = specific humidity at 10 m
q_s = saturation specific humidity
$\bar{Q}_L$ = time-mean zonally-averaged latent heat flux per unit area from the sea surface
$(\bar{Q}_L)_{BAF}$ = value of $\bar{Q}_L$ calculated using the bulk aerodynamic formula
$(\bar{Q}_L)_{GCM}$ = value of $\bar{Q}_L$ calculated in the GCM
r = relative humidity at 10 m
$\bar{r}$ = temporally and zonally averaged value of r
SH = southern hemisphere
SST = sea surface temperature
S_1 = time-mean area-integrated rate of solar energy absorbtion by the ocean basin in zone 1 (average of NH and SH values)
S_2 = as S_1, but for zone 2
T = temperature
T_A = air temperature at 10 m
T_S = sea surface temperature
T_{S1} = area-integrated value of T_S in zone 1
T_{S2} = area-integrated value of T_S in zone 2
u = zonal wind component
u_{10} = value of u at 10 m
$\bar{u}_{10}$ = temporally and zonally averaged value of u_{10}
v = meridional wind component
$\bar{V}$ = time-mean zonally-averaged wind magnitude at 10 m
WVIR = water vapour/infrared radiative (feedback on SST perturbations)
$\bar{Z}_{500}$ = temporally and zonally averaged 500 hPa geopotential height
Z_1 = time-mean area-averaged 500 hPa height in zone 1 (average of NH and SH values)
Z_2 = as Z_1, but for zone 2

$\gamma_{I1} = \partial(F_I)_1/\partial T_{S1}$
$\gamma_{I2} = \partial(F_I)_2/\partial T_{S2}$
$\delta(F_L)_1$ = difference in $(F_L)_1$ between designated experiments
$\delta(F_L)_2$ = difference in $(F_L)_2$ between designated experiments
$\delta\bar{Q}_L$ = difference in $\bar{Q}_L$ between designated experiments
$(\delta\bar{Q}_L)_{BAF}$ = value of $\delta\bar{Q}_L$ calculated using the bulk aerodynamic formula
$(\delta\bar{Q}_L)_{GCM}$ = value of $\delta\bar{Q}_L$ calculated in the GCM
Δq = humidity deficit $(q_s(T_S) - q_A)$
$\Delta\bar{q}$ = temporally and zonally averaged value of Δq
$\Delta T = T_S - T_A$
$\Delta\bar{T}$ = temporally and zonally averaged value of ΔT
$\Delta Z_{500} = Z_1 - Z_2$ (average of NH and SH values)
ρ = surface air density (1.2 kg m^{-3})
τ_x = zonal component of surface stress (of the earth on the atmosphere)
τ_y = meridional component of surface stress (of the earth on the atmosphere)
$\tau = [(\tau_x)^2 + (\tau_y)^2]^{1/2}$
$\bar{\tau}_x$ = temporally and zonally averaged value of τ_x
$\bar{\tau}_y$ = temporally and zonally averaged value of τ_y
$\bar{\tau} = [(\bar{\tau}_x)^2 + (\bar{\tau}_x)^2]^{1/2}$

8. Appendix B

Here we describe the procedure used in calculating the standard error estimates and evaluating the significance of the difference between the means of two data sets. For more detail, the reader is referred to Press et al. (1992), Subsection 14.2.

We estimate the standard error of a set of N measurements $\{x_i\}$ as the standard deviation divided by the square root of N, i.e.,

$$s_D = \sigma/\sqrt{N},$$

where

$$\sigma^2 = \frac{1}{N-1}\sum_{i=1}^{N}(\bar{x} - x_i)^2, \qquad \bar{x} = \frac{1}{N}\sum_{i=1}^{N} x_i.$$

We use the Student t-test for the significance of difference in means, as described in the above reference. If we have two data sets $\{x_i\}$ and $\{y_i\}$, consisting of N_x and N_y measurements, respectively, the standard error of the difference of the means is defined by the formula

$$s = \left[\frac{\sum_{i=1}^{N_x}(\bar{x} - x_i)^2 + \sum_{j=1}^{N_y}(\bar{y} - y_j)^2}{N_x + N_y - 2}\left(\frac{1}{N_x} + \frac{1}{N_y}\right)\right]^{1/2}$$

where

$$\bar{x} = \frac{1}{N_x} \sum_{i=1}^{N_x} x_i, \qquad \bar{y} = \frac{1}{N_y} \sum_{j=1}^{N_y} y_j.$$

The two data sets are significantly different at the 95% confidence level if the difference between $\bar{x}$ and $\bar{y}$ is greater than $2s$.

Typical values of the standard errors for some of the relevant quantities in the 2-year integrations, based on sampling the monthly means ($N = 24$) are:

S (net solar radiation at the surface) — less than 0.01%
F_I (net IR radiative flux at the surface) — about 0.06%
F_L (latent heat flux) — about 0.2%
F_H (sensible heat flux) — about 0.2%
F_M (AM flux) — about 1%
ΔZ_{500} (difference in Z_{500} between the zones) — about 0.2%

9. Appendix C

Feedbacks predicted by the simple model of B99

We here calculate the feedbacks due to the latent, sensible and IR radiative heat fluxes in the simple model of B99 (the notation of that paper will be used in this appendix) for an initial perturbation of $T'_{S1} = T'_{S2} = 2$ K. We also examine the relative contributions of the humidity and wind factors to the evaporative feedbacks for this particular form of initial perturbation.

The perturbation forms of the ocean energy equations are given by eqs. (39) and (40) of B99, i.e.,

$$c_{O1} \frac{dT'_{S1}}{dt} = -[(F_L)'_1 + (F_H)'_1 + (F_I)'_1] - F'_{OH}, \tag{C.1}$$

$$c_{O2} \frac{dT'_{S2}}{dt} = -[(F_L)'_2 + (F_H)'_2 + (F_I)'_2] + F'_{OH}. \tag{C.2}$$

The perturbation flux quantities, linearized about the equilibrium climate, are given by eq. (45) of B99, i.e.,

$$\begin{aligned}&[(F_L)'_1, (F_L)'_2, (F_H)'_1, (F_H)'_2, (F_I)'_1, (F_I)'_2, (F_{OH})']\\ &\quad = [\gamma_{L11}, \gamma_{L21}, \gamma_{H11}, \gamma_{H21}, \gamma_{I1}, 0, \gamma_{O1}]T'_{S1}\\ &\quad + [\gamma_{L12}, \gamma_{L22}, \gamma_{H12}, \gamma_{H22}, 0, \gamma_{I2}, \gamma_{O2}]T'_{S2}.\end{aligned} \tag{C.3}$$

Taking the values of γ_{L11}, etc., from Table 1 of B99 and setting $T'_{S1} = T'_{S2} = 2$ K, (C.3) gives

$$\begin{aligned}&[(F_L)'_1, (F_L)'_2, (F_H)'_1, (F_H)'_2, (F_I)'_1, (F_I)'_2, (F_{OH})']\\ &= [2.44, 0.86, 0.02, 0.04, -0.74, -0.08, 0.28] \text{ PW}.\end{aligned} \tag{C.4}$$

Hence, the combined latent, sensible and IR radiative heat flux tendencies in zones 1 and 2 are

$$[(F_L)'_1 + (F_H)'_1 + (F_I)'_1] = 1.72 \text{ PW}, \tag{C.5}$$

$$[(F_L)'_2 + (F_H)'_2 + (F_I)'_2] = 0.82 \text{ PW}. \tag{C.6}$$

The simple model thus predicts that, in both zones, the latent and sensible heat flux feedbacks will be negative (with the latter small in magnitude), the IR radiative feedback will be positive, and the sum of the latent and sensible heat flux feedbacks will be large enough to overcome the IR radiative feedback.

We note that if we were to include the ocean heat flux feedback $(F_{OH})'$ as determined above in estimating the sign of the overall tendencies given by (C.1) and (C.2), the initial tendencies would still be negative in both zones.

To estimate the relative contributions of the humidity and wind factors to the evaporative feedbacks for the present case ($T'_{S1} = T'_{S2} = 2$ K), we use (C.3) above along with eqs. (41) and (42) of B99 to give

$$\frac{(F_L)'_1}{(\bar{F}_L)_1} = \left[\frac{L}{R_v \bar{T}^2_{S1}} + \frac{a_M(a_{D1} - a_{D2})}{2\bar{F}_M}\right](2 \text{ K}), \tag{C.7}$$

$$\frac{(F_L)'_2}{(\bar{F}_L)_2} = \left[\frac{L}{R_v \bar{T}^2_{S2}} + \frac{a_M(a_{D1} - a_{D2})}{2\bar{F}_M}\right](2 \text{ K}). \tag{C.8}$$

The first terms within the square brackets in (C.7) and (C.8) represent the humidity factor; from B99, their values are 0.060 K^{-1} and 0.070 K^{-1}, respectively. The remaining terms within the square brackets, which are the same for (C.7) and (C.8), represent the wind factor; their value is 0.016 K^{-1}. Thus, for zone 1, the humidity factor accounts for 79% of the evaporative feedback and the wind factor for 21%. The corresponding figures for zone 2 are 81% and 19%, respectively. The simple model thus indicates that for the present form of initial perturbation (but not for all forms of perturbation) both factors have the same sign and the humidity factor dominates in both zones.

REFERENCES

Bates, J. R. 1999. A dynamical stabilizer in the climate system: a mechanism suggested by a simple model. *Tellus* **51A**, 349–372.

Bates, J. R., Moorthi, S. and Higgins, R. W. 1993. A global multilevel atmospheric model using a vector semi-Lagrangian finite difference scheme. Part I: Adiabatic formulation. *Mon. Wea. Rev.* **121**, 244–263.

Bengtsson, L. 1998. A numerical simulation of anthropogenic climate change. In: *The legacy of Svante Arrhenius: Understanding the greenhouse effect* (eds. Rodhe, H. and Charlson, R.). Royal Swedish Academy of Sciences, pp. 127–142.

Cess, R. D., Zhang, M. H., Ingram, W. J., Potter, G. L., Alexeev, V., Barker, H. W., Cohen-Solal, E., Colman, R. A., Dazlich, D. A., Del Genio, A. D., Dix, M. R., Dymnikov, V., Esch, M., Fowler, L. D., Fraser, J. R., Galin, V., Gates, W. L., Hack, J. J., Kiehl, J. T., Le Treut, H., Lo, K. K-W., McAvaney, B. J., Meleshko, V. P., Morcrette, J. J., Randall, D. A., Roeckner, E., Royer, J.-F., Schlesinger, M. E., Sporyshev, P. V., Timbal, B., Volodin, E. M., Taylor, K. E., Wang, W. and Wetherald, R. T. 1996. Cloud feedback in atmospheric general circulation models. An update. *J. Geophys. Res.* **101**, 12,791–12,794.

Chen, M. and Bates, J. R. 1996. A comparison of climate simulations from a semi-Lagrangian and an Eulerian GCM. *J. Climate* **9**, 1126–1149.

Clement, A. C. and Seager, R. 1999. Climate and the tropical oceans. *J. Climate* **12**, in press.

Harshvardhan, Davies, R., Randall, D. A. and Corsetti, T. G. 1987. A fast radiation parameterization for atmospheric circulation models. *J. Geophys. Res.* **92**, 1009–1016.

Helfand, H. M. and Labraga, J. C. 1988. Design of a non-singular level 2.5 second-order closure model for the prediction of atmospheric turbulence. *J. Atmos. Sci.* **45**, 113–132.

Larson, K., Hartmann, D. L. and Klein, S. A. 1999. On the role of clouds, water vapor, circulation and boundary layer structure in the sensitivity of the tropical climate. *J. Climate* **12**, in press.

Lee, W.-H., Iacobellis, S. F. and Somerville, R. C. J. 1997. Cloud radiative forcings and feedbacks: general circulation model tests and observational validation. *J. Climate* **10**, 2479–2496.

Moorthi, S., Higgins, R. W. and Bates, J. R. 1995. A global multilevel atmospheric model using a vector semi-Lagrangian finite difference scheme. Part II: Version with physics. *Mon. Wea. Rev.* **123**, 1523–1541.

Moorthi, S. and Suarez, M. J. 1992. Relaxed Arakawa–Schubert: A parameterization of moist convection for general circulation models. *Mon. Wea. Rev.* **120**, 978–1002.

Press, W. H., Teukolsky, S. A., Vetterling, W. T. and Flannery, B. P. 1992. *Numerical recipes in FORTRAN: the art of scientific computing*, vol. I. Cambridge Univ. Press, 973 pp.

Randall, D. A., Cess, R. D., Blanchet, J. P., Boer, G. J., Dazlich, D. A., Del Genio, A. D., Deque, M., Dymnikov, V., Galin, V., Ghan, S. J., Lacis, A. A., Le Treut, H., Li, Z.-X., Liang, X.-Z., McAvaney, B. J., Meleshko, V. P., Mitchell, J. F. B., Morcrette, J.-J., Potter, G. L., Rikus, L., Roeckner, E., Royer, J. F., Schlese, U., Sheinin, D. A., Slingo, J., Sokolov, A. P., Taylor, K. E., Washington, W. M., Wetherald, R. T., Yagai, I. and Zhang, M.-H. 1992. Intercomparison and interpretation of surface energy fluxes in atmospheric general circulation models. *J. Geophys. Res.* **97**, 3711–3724.

Takacs, L., Molod, A. and Wang, T. 1994. *Documentation of the Goddard earth observing system (GEOS) general circulation model, Version 1*. NASA Tech. Memo. 104606, vol. 1.